

# Mechanisms of Copper-Based Catalyst Deactivation during CO<sub>2</sub> Reduction to Methanol

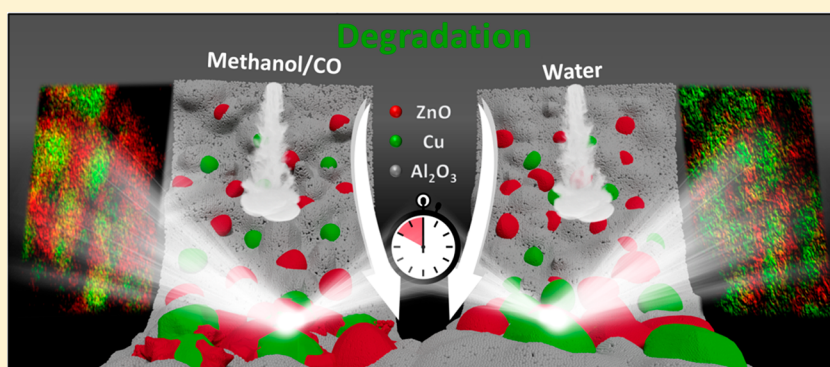
Anže Prašnikar,<sup>\*,†</sup> Andraž Pavličič,<sup>†</sup> Francisco Ruiz-Zepeda,<sup>||</sup> Janez Kovač,<sup>§</sup> and Blaž Likozar<sup>\*,†</sup> 

<sup>†</sup>Department of Catalysis and Chemical Reaction Engineering, National Institute of Chemistry, Hajdrihova 19, 1000 Ljubljana, Slovenia

<sup>||</sup>Department of Materials Chemistry, National Institute of Chemistry, Hajdrihova 19, 1000 Ljubljana, Slovenia

<sup>§</sup>Department of Surface Engineering and Optoelectronics, Jožef Stefan Institute, Jamova 39, 1000 Ljubljana, Slovenia

## Supporting Information



**ABSTRACT:** Despite the fact that the methanol synthesis process includes industrially some of the most important catalytic chemical reactions, it is still not clear how different gaseous species impact catalyst component structure. With the goal to reduce CO<sub>2</sub> emissions through hydrogenation to CH<sub>3</sub>OH, a higher H<sub>2</sub>O formation rate than in the production from compressed CO-rich feed should also be considered. It is known that steam accelerates the sintering of metals, several oxide compounds, and their interfaces. To determine the effect of moisture on the Cu/ZnO/Al<sub>2</sub>O<sub>3</sub> catalysts, a commercial catalytic material was systematically aged at various gas compositions and analyzed using transient H<sub>2</sub> surface adsorption, N<sub>2</sub>O pulse efficient chemisorption, X-ray photoelectron spectroscopy, scanning transmission electron microscopy mapping, X-ray powder diffraction, and N<sub>2</sub> physisorption, and the mechanisms of deactivation were observed. A strong consistent relation between the compacting of Al<sub>2</sub>O<sub>3</sub>, the amount of water in the controlled streamflow, and the activity was found. This connected loss of support resulted in the (re)forming of Cu, ZnO, and Cu/ZnO phases. Copper particle growth was modeled by applying a physical coalescence model. In the presence of CO and/or CH<sub>3</sub>OH, zinc oxide material started to cover the Cu granules, while H<sub>2</sub>O promoted the development of separate Cu regions.

## 1. INTRODUCTION

Methanol is an important chemical for the production of various products such as dimethyl ether, formaldehyde, and acetic acid. Besides being a feedstock chemical, methanol can also be mixed with gasoline and used as a mixture.<sup>1</sup> It can be produced to capture CO<sub>2</sub> emissions from carbon-rich sources such as steel plants and thermoelectric power stations. Conventionally, methanol is synthesized using syn-gas in a packed bed reactor with a recycle at 240–280 °C and 50–100 bar with Cu/ZnO/Al<sub>2</sub>O<sub>3</sub> (CZA) catalyst.

The CZA catalysts are usually used for several years with gradual temperature increase in the reactor to compensate for the activity decrease.<sup>2</sup> Catalysts can be deactivated by particle sintering or sulfur and halogenide poisoning.<sup>3,4</sup> Poisoning is usually eliminated by sulfur/halogenide removal processes;<sup>5,6</sup> however, sintering cannot be simply omitted. The rate of deactivation is usually limited by the addition of refractory

materials (Al<sub>2</sub>O<sub>3</sub>, SiO<sub>2</sub>, MgO, etc.), which act as a support for active components.<sup>7–9</sup>

In addition to the thermal sintering, gas atmosphere can accelerate this process by increasing surface diffusion of the catalyst molecules.<sup>10–12</sup> The surface diffusion of hydroxylated ZnO is faster than that for pure ZnO, resulting in a higher sintering rate.<sup>12</sup> The rate of bulk diffusion is also dependent on the gaseous environment. For example, Gai et al.<sup>13</sup> observed increased diffusion of copper through the alumina layer in the presence of oxygen, which they correlated with surface energy minimization. Recently it was shown, that ZnO grows over Cu particles under the reaction conditions implemented during

**Received:** April 8, 2019

**Revised:** June 28, 2019

**Accepted:** June 29, 2019

**Published:** July 1, 2019

methanol synthesis, resulting in decreased copper surface area.<sup>14,15</sup>

The catalysts for the methanol synthesis were optimized for the conversion of CO-rich syn-gas, however, the deactivation process could proceed differently in the case of pure CO<sub>2</sub> reduction by H<sub>2</sub>. This would be due to larger H<sub>2</sub>O and smaller CO content, since for every molecule of CO<sub>2</sub> an additional molecule of H<sub>2</sub>O is formed. It is widely known that steam increases the sintering rate of oxides and metal particles and therefore decreases active surface area.<sup>9,11,12,16–21</sup>

Steam impacts the catalyst activity temporarily (reversibly) and permanently (irreversibly). Some existing literature has been presented on reversible catalyst deactivation by H<sub>2</sub>O,<sup>22–24</sup> which is caused by occupation of the active sites with \*OH.<sup>24</sup> The rate of methanol formation increases in the presence of CO, which scavenges surface hydroxyls through the water gas shift reaction (WGS). The irreversible deactivation was also studied for Cu/ZnO/ZrO/Al<sub>2</sub>O<sub>3</sub> catalysts with steam being added into the stream,<sup>9,16</sup> indicating that H<sub>2</sub>O increased the rate of deactivation. The rate of deactivation was reduced by the addition of colloid silica, which additionally stabilized the catalyst structure.<sup>9</sup>

However, there was no detailed *post-mortem* catalyst characterization to determine the deactivation mechanism with H<sub>2</sub>O or determination of catalyst morphology changes. For this reason, we performed experiments with the CZA catalyst under different aging compositions at 50 bar and 240 °C for 48 h with the purpose of isolating the effect of H<sub>2</sub>O. The samples after and before aging were analyzed with various techniques to provide a clear picture of structural changes of catalyst samples. The model of H<sub>2</sub>O effect on Cu particle growth is presented. The changes of the catalytic activity were explained by structural transformations.

## 2. EXPERIMENTAL SECTION

To determine the effect of the H<sub>2</sub>O on the methanol catalyst, approximately 400 mg of pelletized commercial Cu/ZnO/Al<sub>2</sub>O<sub>3</sub> catalyst HiFuel W230 (particle sizes 200–400 μm) was inserted into the parallel packed bed reactor system and aged under different conditions. Aging was performed in the same reactor as was used for the catalytic tests. The scheme of parallel packed bed reactor system and filled reactor tube can be found in the Supporting Information, section S6. The catalyst contains 50.2 wt % of CuO, 30.8 wt % of ZnO, and 18.7 wt % of Al<sub>2</sub>O<sub>3</sub> with the addition of graphite as a binder. Before being aged, the samples were reduced in H<sub>2</sub> at 1 bar and 300 °C for 12 h and evaluated in H<sub>2</sub>/CO<sub>2</sub> = 2.5 at 50 bar, 180–240 °C and GHSV 40 000 h<sup>-1</sup> (long form NmL<sub>gas</sub> mL<sub>cat</sub><sup>-1</sup> h<sup>-1</sup>). Catalytic activity was measured again after aging (shown only for 240 °C). In both catalytic tests, catalysts were held at 240 °C for 8 h to ensure that the change in catalyst activity is solely due to the irreversible catalyst changes, for example, alterations due to irreversible catalyst morphology and not from adsorbed species remaining following aging. The samples were transferred and prepared in a glovebox (for the X-ray photoelectron spectroscopy (XPS) and X-ray diffraction (XRD) analyses) or were passivated using N<sub>2</sub>O (for the scanning transmission electron microscopy (STEM), N<sub>2</sub> physisorption, and chemisorption analyses). Figure 1 shows experimental procedure.

Catalytic tests and aging were performed in a parallel reactor system with online gas composition analysis using gas chromatography (Agilent 490 Micro GC, TCD detectors

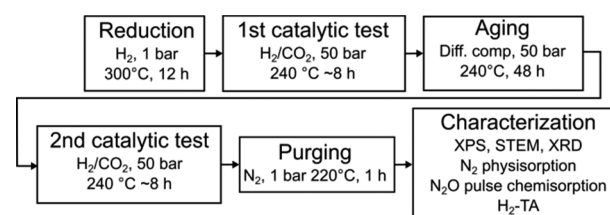


Figure 1. Experimental work procedure.

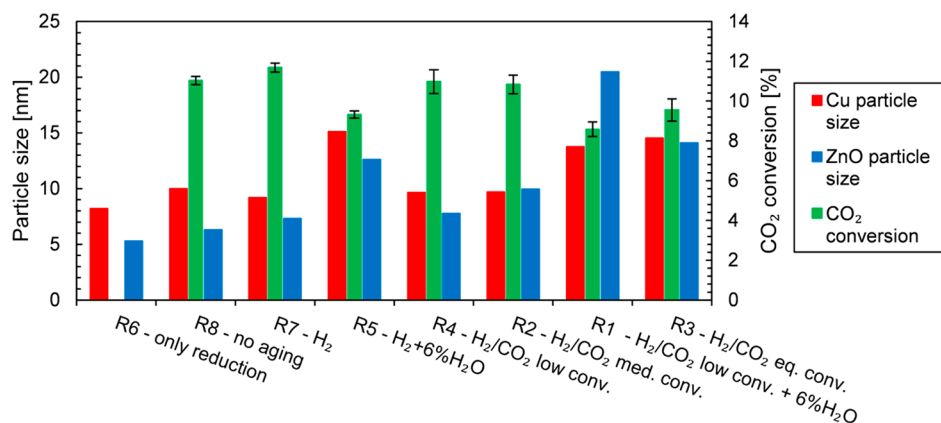
equipped with CP-Molsieve and PoraPlot U columns.). A pre-prepared gas mixture of H<sub>2</sub>/CO<sub>2</sub>/N<sub>2</sub> = 61/29/10 (TPJ, d.o.o., Jesenice) and pure H<sub>2</sub> with purities 99.999% (Messer) were mixed to obtain gas inlet mixtures. In the case of samples R1 and R5, distilled water was pumped with a HPLC pump into the vaporizer where it was mixed with the other gases. The aging conditions and inlet compositions are displayed in Table 1.

Table 1. Catalyst Aging Conditions (Temperature, 240 °C; Pressure, 50 bar)

name	inlet aging gas composition H <sub>2</sub> /CO <sub>2</sub> /H <sub>2</sub> O/N <sub>2</sub>	GHSV [h <sup>-1</sup> ]
R1	62/24.8/5.6/7.6	40 000
R2	65/26/0/8	20 000
R3	65/26/0/8	1 700
R4	65/26/0/8	40 000
R5	93.1/0/6.9/0	40 000
R6	only reduction	
R7	100/0/0/0	13 000
R8	no aging	

The X-ray photoelectron spectroscopy (XPS) analyses were carried out on the PHI-TFA XPS spectrometer produced by Physical Electronics Inc. Sample powders were brought from the catalytic reactor under the protective atmosphere of Ar and introduced into an ultra-high-vacuum spectrometer. The analyzed area was 0.4 mm in diameter and the analyzed depth was about 3–5 nm. Sample surfaces were excited by X-ray radiation from a monochromatic Al source at a photon energy of 1486.6 eV. The high-energy resolution spectra were acquired with a pass energy of 29 eV and an energy resolution of 0.6 eV. Because of the favorable electrical conductivity of the graphite phase involved in the samples, XPS spectra were not aligned since no charging effects were observed. The accuracy of binding energies was about ±0.3 eV. Quantification of surface composition was performed from XPS peak intensities taking into account relative sensitivity factors provided by the instrument manufacturer. Two different XPS measurements were performed on each sample and the average composition was calculated.

Samples for the XRD analyses were powdered and transferred in the inert atmosphere on the XRD holder and covered with the Kapton film. The analyses were performed on the PANalytical X'Pert Pro instrument. The CuKα1 radiation source was used for the scanning from 10° to 90°. Afterward, Rietveld refinement of the XRD patterns was performed to extract the crystal size and phase composition using the *Fm3m*, *P63mc*, and *Fd3m* of Cu, ZnO, and Al<sub>2</sub>ZnO<sub>4</sub> spinel, respectively. The instrumental resolution function was determined by refinement of the XRD pattern of a SiO<sub>2</sub> standard powder. For the fitting procedure, X'Pert HighScore Plus was used with U and W coefficients for description of



**Figure 2.** Particle sizes of Cu (red) and ZnO (blue) determined using XRD by Rietveld refinement. CO<sub>2</sub> conversion (green) is measured after aging at 240 °C, 50 bar, GHSV of 40 000 h<sup>-1</sup>.

**Table 2.** Average Volume Gas Compositions of Aging Gas Mixtures

name		average aging volume fraction [%]					
		H <sub>2</sub>	CO <sub>2</sub>	H <sub>2</sub> O	CO	CH <sub>3</sub> OH	N <sub>2</sub>
R1	H <sub>2</sub> /CO <sub>2</sub> low conv. + 6%H <sub>2</sub> O	61.9	23.8	6.1	0.3	0.1	7.8
R2	H <sub>2</sub> /CO <sub>2</sub> med. conv.	63.4	23.2	2.4	0.9	1.1	9
R3	H <sub>2</sub> /CO <sub>2</sub> eq. conv.	59.1	20	6	1.6	4.5	8.8
R4	H <sub>2</sub> /CO <sub>2</sub> low conv.	64	24	1.9	0.6	1	8.5
R6	H <sub>2</sub> + 6% H <sub>2</sub> O	93.1		6.9			
R7	only reduction						
R8	H <sub>2</sub>	100					
R9	no aging						

*fwhm* peaks. Additionally, anisotropic broadening, asymmetry, and peak shape was also considered for all samples. The background of patterns was described by the iterative method proposed by E. J. Sonneveld and J. W. Visser.<sup>25</sup>

STEM was performed in a Jeol ARM CF probe corrected microscope operated at 200 kV equipped with a SSD Jeol EDX spectrometer. Samples were prepared by sonication in ethanol. A small part of the solution was then drop casted on Ni grids and observed using a microscope.

N<sub>2</sub> physisorption was used to obtain BET specific surface areas. Measurements were performed on Micromeritics ASAP 2020, with the degassing at 200 °C for 17 h with 100 mg of sample. N<sub>2</sub>O pulse chemisorption and H<sub>2</sub>-TA (H<sub>2</sub> transient adsorption) were performed on Micromeritics Autochem II 2920 with 100 mg of catalyst sample. First, to reduce the Cu<sub>2</sub>O layer the samples were purged in H<sub>2</sub> at 240 °C for 30 min, followed by N<sub>2</sub>O pulse chemisorption at 50 °C. The N<sub>2</sub>O gas (Messer) decomposition was monitored with a daily calibrated Pfeiffer Vacuum Thermostar mass spectrometer ( $m/z = 28$  and 30). Following the H<sub>2</sub>-TA, the formed Cu<sub>2</sub>O layer was reduced with 5% H<sub>2</sub>/Ar (Messer) at 40 °C for 1 h. The H<sub>2</sub> uptake was monitored with TCD. Since H<sub>2</sub> is also used for the adsorption on the reduced Cu, we purged the sample in He (Messer) at 220 °C for 1 h to remove the adsorbed H<sub>2</sub> and repeated the H<sub>2</sub>-TA on the reduced samples. The copper surface area was calculated from the differences between H<sub>2</sub> uptake on N<sub>2</sub>O treated and reduced samples.

### 3. RESULTS AND DISCUSSION

The Cu and ZnO particle sizes and CO<sub>2</sub> conversion after different treatments are displayed in Figure 2. Average particle sizes were determined with XRD using Rietveld refinement, while the CO<sub>2</sub> conversions were obtained from the second catalytic tests. Since samples were tested in the parallel reactor system, there are minor differences (<6%) between measured activities at the same conditions. For this reason, results of the second test were normalized using the first catalytic test to more accurately compare samples. The powder diffractograms, weight fractions of crystal phases and particle sizes can be found in the Supporting Information, section 1. As mentioned, catalyst activity can be affected by the adsorbed species which remain on the catalyst surface after aging. To rule out this possibility, catalyst R5 was inserted back into the reactor and treated for 5 h with H<sub>2</sub> at 50 bar and 240 °C. Then the catalytic test was repeated under the same conditions. The catalytic activity of the treated catalyst converged to the same value as that before the treatment.

We choose to show the effects based on gas composition with the average aging gas compositions, since it is the most representative way to cumulatively describe conditions along the catalyst bed. The average aging gas compositions (Table 2) were calculated based on the linear average estimation of measured inlet and outlet fractions. For the sample aged at equilibrium conversion (R3), only the outlet molar fraction was used, since from the additional catalytic tests at 2.4-times higher feed flow (GHSV 4000 1/h) and at the same temperature and pressure, the composition of the outlet gas was the same within the margin of error. Additionally, due to

reactor geometry (cylindrical tube, bed length 11 mm, diameter 6.3 mm) and low linear velocity (0.6 mm/s), the axial dispersion becomes significant, resulting in even more uniform gas composition through the bed length. The amount of water added for the aging of the samples R1 and R5 is nearly equal to the H<sub>2</sub>O formed at the equilibrium conversion of CO<sub>2</sub> and H<sub>2</sub>, without water addition.

**3.1. General Overview of the Aging Impact on the Catalyst.** Aging to a great extent influences particle sizes. The average particle size in the sample without aging (R8) was 10.0 nm for Cu and 6.3 nm for ZnO, while CO<sub>2</sub> conversion was 11%. The comparison with the sample after reduction (R6) demonstrated that catalytic tests do not significantly affect the particle size as Cu and ZnO particle growth were 18% and 16%, respectively. Aging in H<sub>2</sub> (sample R7) also shows only a minor effect on the particle size. It means that the thermal sintering in the reductive atmosphere is not observed in this time frame.

On the other hand, the difference became distinct when the steam was added to the hydrogen gas (sample R5). The average Cu and ZnO particle size increased by 51% and 100% and CO<sub>2</sub> conversion dropped by 15%. H<sub>2</sub>O is responsible for ZnO hydroxylation which increases the surface diffusion and therefore sintering.<sup>19,20</sup> The Cu particle growth might also be explained by the hydroxylation of the surface as for Ni on Al<sub>2</sub>O<sub>3</sub><sup>21</sup> or more likely due to decreased contact between Cu and ZnO and Cu and Al<sub>2</sub>O<sub>3</sub> phases. The contact angle between Cu and ZnO increases in more oxidizing atmospheres,<sup>26,27</sup> which could result in decreased metal–support interaction and therefore faster sintering. Additional discussion on the sintering mechanism can be found in section 3.4.

Water promotes ZnO and Cu particle growth but effects could vary during actual reaction conditions. For this reason, the catalyst was aged in a mixture of H<sub>2</sub>/CO<sub>2</sub> = 2.5 at different residence times (GHSV of 40 000 h<sup>-1</sup> (R4), 20 000 h<sup>-1</sup> (R2), 1700 h<sup>-1</sup> (R3)), and with the addition of water (GHSV of 40,000 h<sup>-1</sup>, R1). R4 and R2 samples at high GHSV both show minor increase in particle size and a low CO<sub>2</sub> conversion decrease, which is in agreement with the work of Sun et al.<sup>2</sup> The addition of water at low CO<sub>2</sub> conversion (sample R1) causes the Cu particle size to increase to a similar size as was observed for the sample without CO<sub>2</sub> in the aging mixture (R5). However, ZnO particles increase by 225% compared to the amount in R8 which is doubled compared to the value obtained from aging without the presence of CO<sub>2</sub> (R5). One possible explanation of the synergistic effect of H<sub>2</sub>O and CO<sub>2</sub> on ZnO growth was given by Varela et al.;<sup>12</sup> H<sub>2</sub>O and CO<sub>2</sub> competitively adsorb on ZnO causing formation of Zn(OH)<sub>2</sub> and ZnCO<sub>3</sub>, respectively. Chemisorption of CO<sub>2</sub> would not significantly increase surface diffusion, but rather increase mobility of ions from the interior to the catalysts surface. The CO<sub>2</sub> conversion has decreased about the same amount as in the case with only water and hydrogen in stream (R5). In the case of aging at equilibrium conversion (sample R3), the volume fraction of water in the aging mixture was approximately the same as for the samples R5 and R1 (~6%). The copper particle size and CO<sub>2</sub> conversion changed almost the same as for the samples R5 and R1, while unexpectedly ZnO particles did not increase as for R1, despite similar concentrations of CO<sub>2</sub> and H<sub>2</sub>O in the stream. Accordingly, some other mechanism connected with the

reaction products could prevent ZnO particle growth, which is discussed below.

From the N<sub>2</sub> physisorption we also obtained average pore size and pore volume (Table S3). The significant pore volume increase of 22% is observed only when the sample aged at equilibrium conversion (R3) is compared to the sample R6. As the pore walls are composed mainly from particles, the average pore size is also related to the particle size as seen in Figure S4.

**3.2. Surface Composition Changes.** To indicate surface composition changes, we calculated the Cu surface fraction and exposed Cu crystallite surface fraction (ECSF<sub>Cu</sub>). The copper surface area was determined using N<sub>2</sub>O pulse chemisorption. The method was validated by H<sub>2</sub> transient adsorption (H<sub>2</sub>-TA) since the N<sub>2</sub>O chemisorption is also used to measure oxygen vacancies.<sup>2</sup> Owing to short reduction time (1 h), the low temperature of reduction (240 °C), and low H<sub>2</sub> partial pressure (0.1 bar), the measured N<sub>2</sub>O uptake is the same as the H<sub>2</sub> uptake from H<sub>2</sub>-TA (in SI, Figure S3). To additionally confirm the above results, we also measured copper surface area of nonreducible support (Cu on Al<sub>2</sub>O<sub>3</sub>) with both methods. The Cu surface areas measured by N<sub>2</sub>O pulse chemisorption and H<sub>2</sub>-TA can be found in Table S2.

We calculated the Cu surface fraction by the ratio of the specific Cu surface area, from the N<sub>2</sub>O pulse chemisorption, with the BET specific surface area (eq 1):

$$\text{Cu surface fraction}[\%] = \frac{S_{\text{Cu}}^{\text{N}_2\text{O}}}{S_{\text{BET}}} \quad (1)$$

Figure 3 shows the dependence of the Cu surface fraction on the CO + MeOH aging fraction. Except for the sample aged at

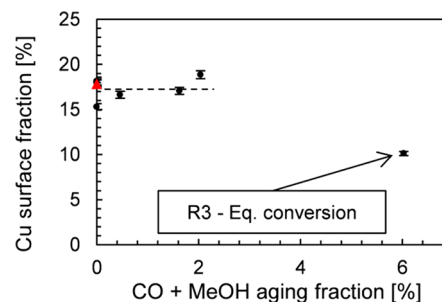


**Figure 3.** Cu fraction on the surface decreases during aging at equilibrium of the conversion, sample R3. The red triangle represents sample R8 (no aging). The line is to guide the eye.

equilibrium conversion (R3), all samples retain almost an equal Cu surface fraction compared to the no aging sample R8 (red triangle), including samples with H<sub>2</sub>O addition. Therefore, at low CO and CH<sub>3</sub>OH content the copper surface area decreases proportionally with BET specific surface area (as seen in Figure 3). Despite large variations regarding (other samples than R3) moisture content, H<sub>2</sub>O does not have a significant effect on this Cu surface fraction. The Cu surface fraction was also estimated with XPS using Cu 2p<sub>3/2</sub>, Zn 2p<sub>3/2</sub>, Al 2p, O 1s, and C 1s peaks. The surface composition was calculated for all analyzed samples and is given in Table S4. The lowest Cu surface fraction is also evident from the ratio of surface coverage [Cu]/[Cu + Zn + Al] obtained from XPS (Figure 4). It should be noted that this is a ratio of fractions in atomic percentages.

One possible reason of the lowering of the Cu surface fraction is the ZnO covering of the Cu particle.<sup>14,15,28</sup> To

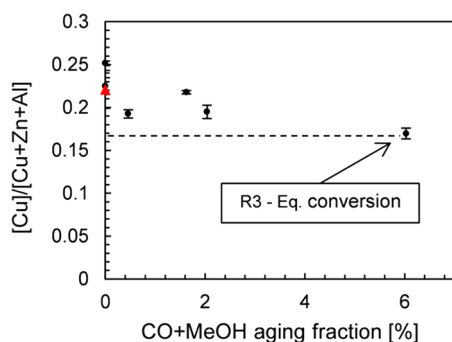


**Figure 4.** Cu surface fraction obtained by XPS depending on the aging of the CO + CH<sub>3</sub>OH fraction. The red triangle represents sample R8 (no aging).

indicate the Cu overlay, we calculated the exposed Cu crystallite surface fraction:

$$\text{ECSF}_{\text{Cu}} [\%] = \frac{S_{\text{Cu}}^{\text{N}_2\text{O}}}{S_{\text{Cu}}^{\text{XRD}}} 100; S_{\text{Cu}}^{\text{XRD}} = \frac{6L_{\text{Cu}}}{\rho_{\text{Cu}} d_{\text{Cu}}^{\text{XRD}}} \quad (2)$$

where  $S_{\text{Cu}}^{\text{XRD}}$  represents the surface of Cu crystallites, which is calculated using copper crystallite size  $d_{\text{Cu}}^{\text{XRD}}$ , copper loading ( $L_{\text{Cu}} = 0.277 \text{ g}_{\text{Cu}}/\text{g}_{\text{cat}}$ ), and copper density (8.92 g/mL), assuming spherical crystallite shape. The  $\text{ECSF}_{\text{Cu}}$  is the lowest (37%) for sample R3, while the values for other samples are in the range of  $51 \pm 6\%$  (Figure 5). Therefore H<sub>2</sub>O does not

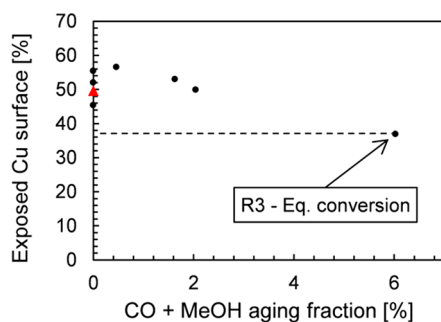


**Figure 5.** Exposed Cu surface fraction ( $\text{ECSF}_{\text{Cu}}$ ) calculated from the ratio of specific surface area measured with N<sub>2</sub>O and theoretical specific surface area of Cu crystallites. The red triangle represents sample R8 (no aging).

promote Cu overgrowth, in fact the samples with H<sub>2</sub>O addition (R1 and R5) expose the highest  $\text{ECSF}_{\text{Cu}}$  (57% and 55%, respectively). Additionally, the STEM-EDX mapping (Figure 6) clearly shows that for the sample R3, the ZnO phase is much more spread over the Cu phase, as compared to samples R1 and R6 (see also Supporting Information).

**3.3. Catalytic Activity Changes.** Catalytic activity is frequently reported to be proportionally correlated to Cu surface area;<sup>29,30</sup> however, in our case we can see only a weak relation of conversion and metal surface area (Figure 7).

The turnover frequency ( $\text{TOF}_{\text{CO+MeOH}}$ ) was calculated to estimate the effect of aging conditions on the specific activity. The activities from the second catalytic test at 240 °C and 50 bar were used and normalized to  $S_{\text{Cu}}$  from N<sub>2</sub>O pulse chemisorption. As previously mentioned, only the copper surface area without ZnO<sub>x</sub> oxygen vacancies was measured by N<sub>2</sub>O pulse chemisorption. As shown in Figure 8, aging does not significantly impact the TOF except for the sample aged at

equilibrium conversion (R3) where it increases. Simultaneously, sample R3 also exhibits the lowest  $\text{ECSF}_{\text{Cu}}$  and the highest surface Zn/Cu ratio (Figure 9), indicating the covering of Cu with ZnO and increasing specific activity.

The change of TOF is not correlated to the Cu particle size since the sizes of R3 and R5 are nearly the same (14.5 and 15.1 nm, respectively), while the TOF differs by 50% (0.06 and 0.089 1/s, respectively). In the work by van den Berg et al.<sup>31</sup> it was shown that TOF is constant for the particles larger than 8 nm, which are smaller particles than observed in this work.

The same result was obtained by Fichtl et al.<sup>16</sup> where TOF for methanol increased during the first 200 h for the catalyst aged at equilibrium conversion. This behavior cannot be explained by the change of Cu particle size, since the specific activity (TOF) is almost constant for the Cu particles larger than 10 nm.<sup>31</sup> However, by STEM-EDX (Figure 6) and factor  $\text{ECSF}_{\text{Cu}}$  (Figure 9) it can be observed that the ZnO covers the Cu surface and promotes specific catalyst activity. The activity increase was also reported for Cu(111) covered by ZnO, with the maximum activity at 20% Cu(111) covered by ZnO.<sup>32,33</sup> Fichtl et al.<sup>16</sup> found actual increase in the activity for the catalyst aged at equilibrium conditions at 220 °C in the first 50 h. Owing to similar conditions, ZnO could similarly overlay the surface of Cu and increase the overall catalyst activity. However, in our case we did not observe the increase of overall catalytic activity (as seen in Figure 2), but it was observed in the first 10 h of the stability test at 50 bar (Figure S11). Therefore, too much of the ZnO overlayer can be formed, and this can decrease the catalyst activity which was also indicated by Lunkenbein et al.<sup>15</sup> The impact on the methanol selectivity is insignificant with the minimum selectivity of 60% for the sample R1 and maximum selectivity of 62% for sample R4. The  $\text{TOF}_{\text{CO+MeOH}}$  in the experiments with the water addition (R1 and R5) were nearly the same as in the case of aging at low conversion. In contrast, Fichtl et al.<sup>16</sup> observed a steep decrease in specific activity when 10% of the steam was added for 12 h at 220 °C and 60 bar. The difference could come from the fact that the catalyst was further aged at equilibrium conditions, resulting in increased sintering due to loss of Al<sub>2</sub>O<sub>3</sub> support for Cu and ZnO. Deactivation by coking is dismissed due to the carbon phase surface fraction ranging between 30% and 36% (Table S6) for all samples and is in the range of the repeatability of analyses.

**3.4. Modeling of the H<sub>2</sub>O Influence on Cu Particle Growth.** Sintering of the catalyst can proceed by several ways. Herein two of the most probable mechanisms will be presented. First is the coalescence mechanism which is caused by the increased particle migration by weaker contact between the metal and support or increased surface diffusion of catalytic material. The other important mechanism is Ostwald ripening which is caused by the surface diffusion of catalytic material and higher thermodynamic stability of larger particles.<sup>16,34</sup> Early in the process of sintering, particles would likely sinter by a coalescence mechanism since they are already in contact, while in the end phase of sintering, the particles can undergo the Ostwald ripening mechanism.<sup>35</sup> Fichtl et al.<sup>16</sup> modeled the catalyst deactivation and found out that the particle migration model describes the particle size distribution the best. For the reasons stated above, and because these deactivation studies were conducted at short aging times, the coalescence model was chosen.

The addition of Al<sub>2</sub>O<sub>3</sub> to Cu/ZnO catalyst strongly enhances the catalyst stability.<sup>7</sup> The state of Al<sub>2</sub>O<sub>3</sub> has

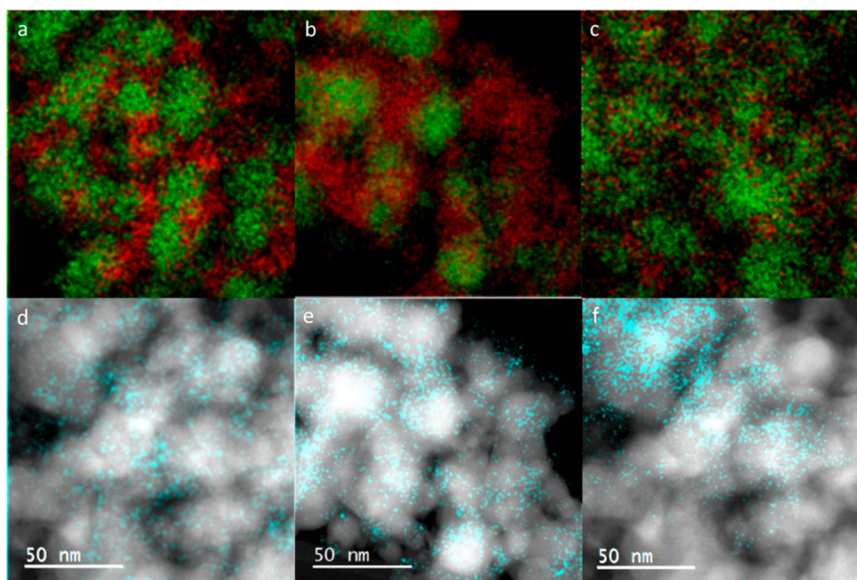


**Figure 6.** AC-STEM ADF images with corresponding EDX signal for Cu (green), Zn (red), and 4Al (blue) of samples R1 (low conversion + H<sub>2</sub>O (a,d)), R3 (equilibrium conversion (b,e)) and R6 (after reduction (c,f)).

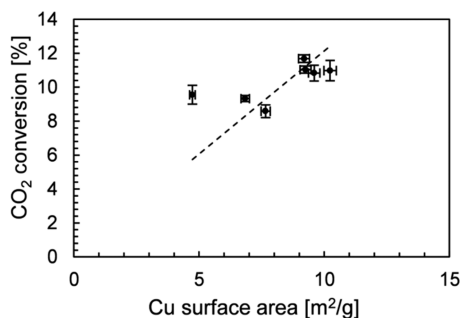


**Figure 7.** CO<sub>2</sub> conversion after aging as a function of Cu surface area. Reaction conditions  $T = 240\text{ }^{\circ}\text{C}$ ,  $p = 50\text{ bar}$ , GHSV = 40 000 h<sup>-1</sup>. The dashed line represents proportional correlation between the Cu surface area and CO<sub>2</sub> conversion.

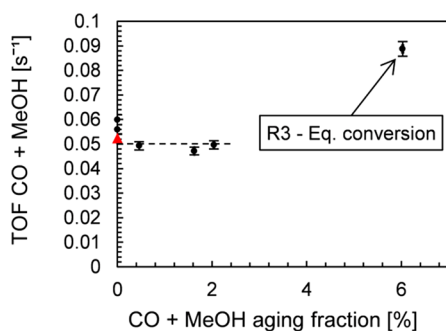


**Figure 8.** Sum of CO and CH<sub>3</sub>OH turnover frequency of the Cu surface (black circles). Activity measurement conditions: 240 °C, 50 bar, and GHSV of 40 000 h<sup>-1</sup>. The red triangle denotes sample R8 (no aging).

therefore detrimental impact on the sintering behavior of the Cu and ZnO phase and it could change in the presence of water. In the presence of large amounts of steam, the catalyst stability can be additionally increased using SiO<sub>2</sub>,<sup>9</sup> thus doping a commercial CZA material. The Al<sub>2</sub>O<sub>3</sub> phase is therefore sensitive to the moisture content. From the images acquired with STEM-EDX for the samples R1, R3, and R6, we observe

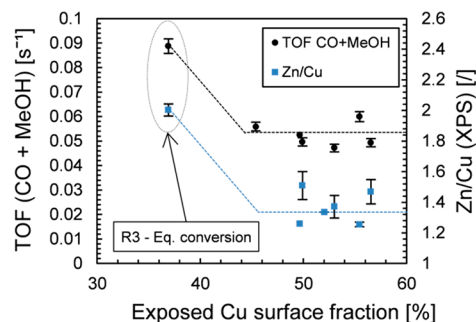


**Figure 9.** Sum of CO and MeOH turnover frequency and Zn/Cu ratio determined by XPS as a function of exposed Cu surface fraction. Activity measurement conditions: 240 °C, 50 bar and GHSV of 40 000 h<sup>-1</sup>. The dashed lines are guides to the eye.

that small Al<sub>2</sub>O<sub>3</sub> particles uniformly cover Cu and ZnO phase. These small particles could decrease the mobility of the Cu and ZnO phases. In all studies with aging (in the presence of H<sub>2</sub>O and/or CO<sub>2</sub>), we observe the formation of 7–10% of a Zn-spinel phase (Al<sub>2</sub>ZnO<sub>4</sub>) with a particle size between 7 and 15 nm (Table S1). A portion of Al<sub>2</sub>O<sub>3</sub> (~25%) is therefore consumed during the formation of Zn-spinel, while the other Al<sub>2</sub>O<sub>3</sub> species could be unavailable due to agglomeration. The peak for the crystalline Al<sub>2</sub>O<sub>3</sub> was not observed in any XRD diffractogram as in the long term study by Lunkenbein et al.<sup>15</sup> To monitor the state of Al<sub>2</sub>O<sub>3</sub>, the surface area of Al from XPS and BET surface area (section 4.1). Since only a minor part of Al<sub>2</sub>O<sub>3</sub> is incorporated in a spinel, the entire Al is represented as Al<sub>2</sub>O<sub>3</sub>. To validate the approach of the combination of XPS and BET, the Cu<sub>2</sub>O surface area from the XPS is plotted against the Cu surface area determined from N<sub>2</sub>O pulse chemisorption (Figure S7). In Figure 10, Cu particle size, ZnO particle size, and Al<sub>2</sub>O<sub>3</sub> surface area are displayed as a function of aging molar fractions of H<sub>2</sub>O. It can be observed that all phases exhibit a decrease in surface area (or increase of particle size) with increasing amount of steam. The sample R8 shows nearly identical features as sample R4, indicating that all catalyst

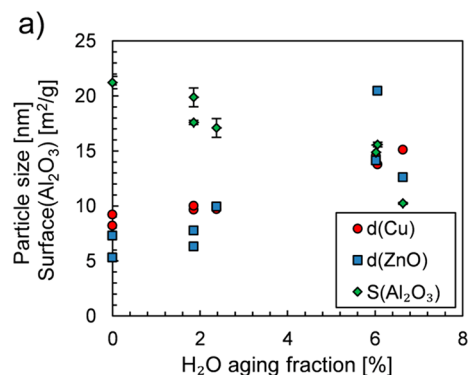


**Figure 10.** H<sub>2</sub>O impact on the Cu and ZnO particle size and on the Al<sub>2</sub>O<sub>3</sub> surface.

sintering occurred in the first 16 h (at 240 °C) and for this reason is plotted at the same H<sub>2</sub>O fraction. The S(Al<sub>2</sub>O<sub>3</sub>)- $x$ (H<sub>2</sub>O) and  $d$ (Cu)- $x$ (H<sub>2</sub>O) relations are very simple despite different aging conditions. The ZnO particle size is much more dependent from other parameters as was discussed in the section 3.2.

From the observed experimental data and literature review, it is now possible to critically discuss the proposed mechanisms of the H<sub>2</sub>O effect on the catalyst. The hydroxylation of Cu could increase surface diffusion of the metal particle and therefore sintering as for the case with Ni.<sup>21</sup> H<sub>2</sub>O can adsorb on the Cu surface and dissociate to form adsorbed hydroxyl and hydrogen. The presence of surface H<sub>2</sub>O was proven during methanol synthesis by DRIFT.<sup>36,37</sup> Residual \*OH is also present on the surface, after the ratio between CO<sub>2</sub> and CO decrease.<sup>24</sup> Adsorbed H<sub>2</sub>O/\*OH could increase the surface diffusion of Cu and subsequently cause Cu particle growth. However, H<sub>2</sub>O adsorbs much stronger on the Al<sub>2</sub>O<sub>3</sub> and ZnO surface and can also hydroxylate them to form AlOOH and Zn(OH)<sub>2</sub>, respectively. As mentioned, Zn(OH)<sub>2</sub> has a larger surface diffusion than ZnO and can be therefore sintered faster. Another mechanism discussed in literature is that under relatively oxidizing atmospheres, Cu-ZnO interactions weaken,<sup>26,27</sup> which could promote Cu crystallite growth. However, the loss of the metal-support interaction due to a much higher increase of ZnO particle size in the case of R1 (20.5 nm) comparing to R5 (12.6 nm), also does not have any significant effect on the Cu particle growth ( $d_{Cu}$  = 13.8 nm (R1), 15.1 nm (R5)). Despite the ZnO overlay over the Cu particles (R3), the Cu particle size still increases by approximately the same amount ( $d_{Cu}$  = 14.5 nm (R3)).

Since the Al<sub>2</sub>O<sub>3</sub> limits the sintering of other more mobile phases, the most probable catalyst deactivation mechanism with water is due to a loss of Al<sub>2</sub>O<sub>3</sub> surface and consequently decrease of Cu and ZnO support. From XPS measurements we estimated that Al<sub>2</sub>O<sub>3</sub> is the most abundant phase on the catalytic surface (50–60%, Table S6). Additionally, TEM images show small particles of Al<sub>2</sub>O<sub>3</sub> finely dispersed over Cu and ZnO (Figure 6). The Cu particle growth is closely correlated with the decrease of the Al<sub>2</sub>O<sub>3</sub> surface (Figure 11).

In line with our observations and the above-mentioned literature, we state that the rate determining step is the decrease of available Al<sub>2</sub>O<sub>3</sub> for the support of Cu phase. The decrease of support is correlated to the loss of Al<sub>2</sub>O<sub>3</sub> surface and therefore the amount of steam in the aging atmosphere. A model for Ni particle growth in the presence of steam<sup>21</sup> is modified and implemented. The surface diffusivity of Ni(OH)<sub>2</sub>

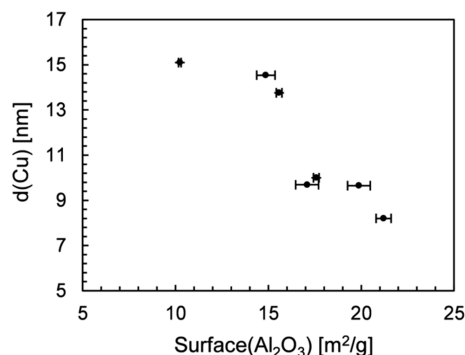


**Figure 11.** Relation between Al<sub>2</sub>O<sub>3</sub> surface and Cu particle size.

is faster than for Ni, which is responsible for increased Ni growth. Due to the discussed similarity between the systems, their modified model for Ni particle growth is used (eq 3):

$$\frac{d_{Cu}}{d_{Cu}^0} = (1 + kt x_{H_2O}^m)^{1/(n-1)} \quad (3)$$

where  $d_{Cu}$  is Cu particle size,  $d_{Cu}^0$  is the initial crystallite size,  $k$  is the growth rate constant,  $t$  is time,  $x$  is H<sub>2</sub>O molar fraction,  $m$  represents the nonlinearity of the atmosphere effect on sintering, and  $n$  is related to the growth mechanism.<sup>21</sup> For the particle migration and coalescence,  $n$  is 8.<sup>21</sup> To isolate sintering due to H<sub>2</sub>O, the Cu particle size of the sample sintered in H<sub>2</sub> (R7) is used as  $d_{Cu}^0$ .

In Figure 12, Cu particle growth is plotted as a dependence of H<sub>2</sub>O molar fraction. In the figure we show that the model

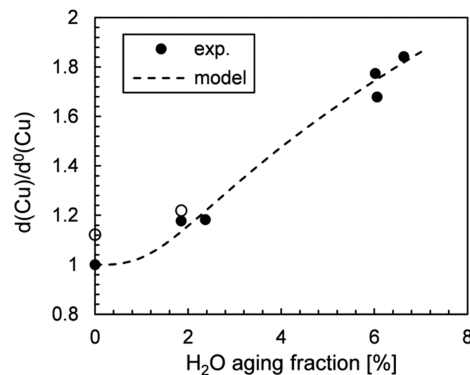


**Figure 12.** Growth factor for Cu ( $d_{Cu}/d_{Cu}^0$ ) depending on the molar fraction of the water and model results for 48 h. The samples R6 and R8 (empty circles) were not included in the regression due to a different aging time.

for  $k$  is  $0.56 \text{ s}^{-1}$  and  $m$  is 3. However, with the change of  $k$  it is also possible to use  $m$  between 3 and 5 to obtain sufficient fit. Number  $m$  is larger than 1, which is an indication that Al<sub>2</sub>O<sub>3</sub> sinter faster (and therefore also Cu) when there are neighboring Al<sub>2</sub>O<sub>3</sub> influenced by H<sub>2</sub>O.

#### 4. CONCLUSION

In the synthesis of methanol from CO<sub>2</sub>, an equivalent amount of water is also produced. To obtain the impact of water on the methanol catalyst, we performed aging experiments at various gas compositions and *post-mortem* analysis of samples using different methods. We concluded that the most probable cause of catalyst deactivation is increasing the rate of sintering of Al<sub>2</sub>O<sub>3</sub> with water. The Al<sub>2</sub>O<sub>3</sub> surface decreases with increasing

molar fraction of H<sub>2</sub>O, while similar trends also follow the growth of the Cu particle size. The Cu particle growth was also fitted to a coalescence model for sintering. While the form of Cu and the Al<sub>2</sub>O<sub>3</sub> phase shows simple dependence on the amount of H<sub>2</sub>O in a gas stream, the ZnO particle size is also dependent on other reaction products and CO<sub>2</sub> in addition to H<sub>2</sub>O. With various methods we confirm that under aging in the presence of large amounts of reaction products (CO, CH<sub>3</sub>OH), the ZnO phase starts to cover Cu particles. In contrast, water promotes the growth of each individual phase.

## ■ ASSOCIATED CONTENT

### ■ Supporting Information

The Supporting Information is available free of charge on the ACS Publications website at DOI: 10.1021/acs.iecr.9b01898.

Rietveld refinement results, XRD diffractograms, validation of N<sub>2</sub>O pulse chemisorption method, pore size distribution and pore volume, determination of surface composition using XPS including estimation of Al<sub>2</sub>O<sub>3</sub> surface area and verification using N<sub>2</sub>O pulse chemisorption, HRTEM images, parallel reactor system scheme, long-term catalytic test (PDF)

## ■ AUTHOR INFORMATION

### ■ Corresponding Authors

\*E-mail: [blaz.likozar@ki.si](mailto:blaz.likozar@ki.si)

\*E-mail: [anze.prasnikar@ki.si](mailto:anze.prasnikar@ki.si)

### ■ ORCID

Blaž Likožar: 0000-0001-9194-6595

### ■ Notes

The authors declare no competing financial interest.

## ■ ACKNOWLEDGMENTS

This research was supported by Slovenian Research Agency (Research Core Funding No. P2 0152) and Project FReSMe No 727504. The authors are very grateful to Urška Kavčič for N<sub>2</sub> physisorption measurements, Brett Pomeroy for language editing, and Matic Grom for the scheme and help with reactor operation.

## ■ REFERENCES

- (1) Olah, G. A. Beyond Oil and Gas: The Methanol Economy. *Angew. Chem., Int. Ed.* **2005**, *44*, 2636–2639.
- (2) Sun, J. T.; Metcalfe, I. S.; Sahibzada, M. Deactivation of Cu/ZnO/Al<sub>2</sub>O<sub>3</sub> Methanol Synthesis Catalyst by Sintering. *Ind. Eng. Chem. Res.* **1999**, *38*, 3868–3872.
- (3) Forzatti, P.; Lietti, L. Catalyst Deactivation. *Catal. Today* **1999**, *52*, 165–181.
- (4) Arcidiacono, S.; Bieri, N. R.; Poulidakos, D.; Grigoropoulos, C. P. On the Coalescence of Gold Nanoparticles. *Int. J. Multiphase Flow* **2004**, *30*, 979–994.
- (5) Kung, H. H. Deactivation of Methanol Synthesis Catalyst-A Review. *Catal. Today* **1992**, *11*, 443–453.
- (6) Hochgesand, G. Rectisol and Purisol. *Ind. Eng. Chem.* **1970**, *62*, 37–43.
- (7) Kurtz, M.; Wilmer, H.; Genger, T.; Hinrichsen, O.; Muhler, M. Deactivation of Supported Copper Catalysts for Methanol Synthesis. *Catal. Lett.* **2003**, *86*, 77–80.
- (8) Twigg, M. V.; Spencer, M. S. Deactivation of Supported Copper Metal Catalysts for Hydrogenation Reactions. *Appl. Catal., A* **2001**, *212*, 161–174.

- (9) Wu, J.; Saito, M.; Takeuchi, M.; Watanabe, T. The Stability of Cu/ZnO-Based Catalysts in Methanol Synthesis from a CO<sub>2</sub>-Rich Feed and from a CO-Rich Feed. *Appl. Catal., A* **2001**, *218*, 235–240.
- (10) Simonsen, S. B.; Chorkendorff, I.; Dahl, S.; Skoglundh, M.; Sehested, J.; Helveg, S. Direct Observations of Oxygen-Induced Platinum Nanoparticle Ripening Studied by In Situ TEM. *J. Am. Chem. Soc.* **2010**, *132*, 7968–7975.
- (11) Challa, S. R.; Delariva, A. T.; Hansen, T. W.; Helveg, S.; Sehested, J.; Hansen, P. L.; Garzon, F.; Datye, A. K. Relating Rates of Catalyst Sintering to the Disappearance of Individual Nanoparticles during Ostwald Ripening. *J. Am. Chem. Soc.* **2011**, *133*, 20672–20675.
- (12) Varela, J. A.; Whittemore, O. J.; Longo, E. Pore Size Evolution during Sintering of Ceramic Oxides. *Ceram. Int.* **1990**, *16*, 177–189.
- (13) Gal, P. L.; Smith, B. C.; Owen, G. Bulk Diffusion of Metal Particles on Ceramic Substrates. *Nature* **1990**, *348*, 430–432.
- (14) Schumann, J.; Kröhnert, J.; Frei, E.; Schlögl, R.; Trunschke, A. IR-Spectroscopic Study on the Interface of Cu-Based Methanol Synthesis Catalysts: Evidence for the Formation of a ZnO Overlayer. *Top. Catal.* **2017**, *60*, 1735–1743.
- (15) Lunkenbein, T.; Girgsdies, F.; Kandemir, T.; Thomas, N.; Behrens, M.; Schlögl, R.; Frei, E. Bridging the Time Gap: A Copper/Zinc Oxide/Aluminum Oxide Catalyst for Methanol Synthesis Studied under Industrially Relevant Conditions and Time Scales. *Angew. Chem., Int. Ed.* **2016**, *55*, 12708–12712.
- (16) Fichtl, M. B.; Schlereth, D.; Jacobsen, N.; Kasatkin, I.; Schumann, J.; Behrens, M.; Schlögl, R.; Hinrichsen, O. Kinetics of Deactivation on Cu/ZnO/Al<sub>2</sub>O<sub>3</sub> Methanol Synthesis Catalysts. *Appl. Catal., A* **2015**, *502*, 262–270.
- (17) Twigg, M. V.; Spencer, M. S. Deactivation of Copper Metal Catalysts for Methanol Decomposition, Methanol Steam Reforming and Methanol Synthesis. *Top. Catal.* **2003**, *22*, 191–203.
- (18) Hansen, T. W.; Delariva, A. T.; Challa, S. R.; Datye, A. K. Sintering of Catalytic Nanoparticles: Particle Migration or Ostwald Ripening? *Acc. Chem. Res.* **2013**, *46*, 1720–1730.
- (19) Borgwardt, R. H. Calcium Oxide Sintering in Atmospheres Containing Water and Carbon Dioxide. *Ind. Eng. Chem. Res.* **1989**, *28*, 493–500.
- (20) Dargatz, B.; Gonzalez-Julian, J.; Bram, M.; Jakes, P.; Besmehn, A.; Schade, L.; Röder, R.; Ronning, C.; Guillon, O. FAST/SPS Sintering of Nanocrystalline Zinc Oxide — Part I: Enhanced Densification and Formation of Hydrogen-Related Defects in Presence of Adsorbed Water. *J. Eur. Ceram. Soc.* **2016**, *36*, 1207–1220.
- (21) Sehested, J.; Gelten, J. A. P.; Helveg, S. Sintering of Nickel Catalysts: Effects of Time, Atmosphere, Temperature, Nickel-Carrier Interactions and Dopants. *Appl. Catal., A* **2006**, *309*, 237–246.
- (22) Sahibzada, M.; Metcalfe, I. S.; Chadwick, D. Methanol Synthesis from CO/CO<sub>2</sub>/H<sub>2</sub> over Cu/ZnO/Al<sub>2</sub>O<sub>3</sub> at Differential and Finite Conversions. *J. Catal.* **1998**, *174*, 111–118.
- (23) Liu, G.; Willcox, D.; Garland, M.; Kung, H. H. The Role of CO<sub>2</sub> in Methanol Synthesis on Cu-Zn Oxide: An Isotope Labeling Study. *J. Catal.* **1985**, *96*, 251–260.
- (24) Martin, O.; Pérez-Ramírez, J. New and Revisited Insights into the Promotion of Methanol Synthesis Catalysts by CO<sub>2</sub>. *Catal. Sci. Technol.* **2013**, *3*, 3343–3352.
- (25) Sonneveld, E. J.; Visser, J. W. Automatic Collection of Powder Data from Photographs. *J. Appl. Crystallogr.* **1975**, *8*, 1–7.
- (26) Grunwaldt, J.-D.; Molenbroek, A. M.; Topsøe, N.-Y.; Topsøe, H.; Clausen, B. S. In Situ Investigations of Structural Changes in Cu/ZnO Catalysts. *J. Catal.* **2000**, *194*, 452–460.
- (27) Hansen, P. L.; Wagner, J. B.; Helveg, S.; Rostrup-Nielsen, J. R.; Clausen, B. S.; Topsøe, H. Atom-Resolved Imaging of Dynamic Shape Changes in Supported Copper Nanocrystals. *Science* **2002**, *295*, 2053–2055.
- (28) Kuld, S.; Conradsen, C.; Moses, P. G.; Chorkendorff, I.; Sehested, J. Quantification of Zinc Atoms in a Surface Alloy on Copper in an Industrial-Type Methanol Synthesis Catalyst. *Angew. Chem., Int. Ed.* **2014**, *53*, S941–S945.

(29) Natesakhawat, S.; Lekse, J. W.; Baltrus, J. P.; Ohodnicki, P. R.; Howard, B. H.; Deng, X.; Matranga, C. Active Sites and Structure-Activity Relationships of Copper-Based Catalysts for Carbon Dioxide Hydrogenation to Methanol. *ACS Catal.* **2012**, *2*, 1667–1676.

(30) Zhan, H.; Li, F.; Gao, P.; Zhao, N.; Xiao, F.; Wei, W.; Sun, Y. Influence of Element Doping on La-Mn-Cu-O Based Perovskite Precursors for Methanol Synthesis from CO<sub>2</sub>/H<sub>2</sub>. *RSC Adv.* **2014**, *4*, 48888–48896.

(31) van den Berg, R.; Prieto, G.; Korpershoek, G.; van der Wal, L. I.; van Bunningen, A. J.; Lægsgaard-Jørgensen, S.; de Jongh, P. E.; de Jong, K. P. Structure Sensitivity of Cu and CuZn Catalysts Relevant to Industrial Methanol Synthesis. *Nat. Commun.* **2016**, *7*, 1–7.

(32) Kattel, S.; Ramirez, P. J.; Chen, J. G.; Rodriguez, J. A.; Liu, P. Active Sites for CO Hydrogenation to Methanol on Cu/ZnO Catalysts. *Science* **2017**, *355*, 1296–1299.

(33) Palomino, R. M.; Ramirez, P. J.; Liu, Z.; Hamlyn, R.; Waluyo, I.; Mahapatra, M.; Orozco, I.; Hunt, A.; Simonovis, J. P.; Senanayake, S. D.; Rodriguez, J. A. Hydrogenation of CO on ZnO/Cu(100) and ZnO/Cu(111) Catalysts: Role of Copper Structure and Metal - Oxide Interface in Methanol Synthesis. *J. Phys. Chem. B* **2018**, *122*, 794–800.

(34) An, B.; Zhang, J.; Cheng, K.; Ji, P.; Wang, C.; Lin, W. Confinement of Ultrasmall Cu/ZnOx Nanoparticles in Metal-Organic Frameworks for Selective Methanol Synthesis from Catalytic Hydrogenation of CO. *J. Am. Chem. Soc.* **2017**, *139*, 3834–3840.

(35) Bartholomew, C. H. Mechanisms of Catalyst Deactivation. *Appl. Catal., A* **2001**, *212*, 17–60.

(36) Yang, R.; Fu, Y.; Zhang, Y.; Tsubaki, N. In Situ DRIFT Study of Low-Temperature Methanol Synthesis Mechanism on Cu/ZnO Catalysts from CO-Containing Syngas Using Ethanol Promoter. *J. Catal.* **2004**, *228*, 23–35.

(37) Fisher, I. A.; Bell, A. T. In-Situ Infrared Study of Methanol Synthesis from H<sub>2</sub>/CO. *J. Catal.* **1997**, *172*, 222–237.